



Effects of moisture and electrode material on AlN-based resistive random access memory

Hee Ju Yun, Byung Joon Choi*

Department of Materials Science and Engineering, Seoul National University of Science and Technology (Seoultech), Seoul, 01811, South Korea



ARTICLE INFO

Keywords:

Resistive random access memory
AlN
Moisture
Electrode material
Degradation

ABSTRACT

Resistive random access memory (RRAM) has been developed as a next-generation nonvolatile memory because of its fast operation speed, low power consumption, high density, and simple structure. Non-oxide materials such as AlN-based RRAM also exhibit low operation energy and large on/off ratios. However, AlN-based RRAM may deteriorate upon oxidation when exposed to air/moisture. In addition, chemical reactivity between the electrode and the switching layer material affects device stability. In this study, four kinds of top electrode materials (Al, Ti, TiN, and Pt) were used in an AlN/TiN stack and a water-resistant encapsulation layer was used to prevent the degradation of AlN-based RRAM. The electrical properties of the device were measured at weekly intervals for 7 weeks. The devices containing Al and Ti top electrodes showed degradation of resistance states despite being encapsulated in a thin Al₂O₃ layer. In contrast, the devices with TiN and Pt electrodes maintained their resistance states and switching properties regardless of the encapsulation layer. These trends in degradation can be explained by the electrode and AlN reactivity with moisture based on fundamental thermodynamics.

1. Introduction

Resistive random access memory (RRAM) is a non-volatile memory that stores digital data based on resistive switching phenomena [1,2]. Various materials have been studied for use as resistive switching layers. In particular, AlN exhibits a wide band gap energy (6.2 eV) and high thermal conductivity (285 W/m·K), which are beneficial for reducing the operating current and local heating [3]. Pt-free Al/AlN/TiN-based RRAM exhibits a pinched hysteresis loop similar to that of Al/AlN/Pt devices with low switching currents [4,5]. It has been reported that the conduction channel composed of nitrogen vacancies (V_N^{3+}) is responsible for resistive switching in AlN-based systems according to electrical measurements and transmission electron microscopy (TEM) observations [5].

Moisture or oxygen-related defects affect RRAM device performance because they can be reduced at the metal/oxide interface or create charge-trapping sites [6–10]. In the oxide-based resistive systems, higher partial pressures of water resulted in lower forming voltages and higher conductivities [8–10]. Nitride-based resistive switching systems are also affected by moisture and oxygen. Oxygen ions can be substituted for nitrogen in the AlN, as predicted by fundamental thermodynamics [11,12]. Moisture can incorporate into the film as an impurity during the deposition process or experimental measurements [10,13].

Similarly, moisture may form oxides in the nitride film and create an interfacial layer at the metal/nitride interface. Therefore, AlN-based RRAM can be easily degraded by moisture or oxygen incorporation. An effective method for preventing the incorporation of external oxygen and moisture is encapsulation of the device in a water-resistant layer such as Al₂O₃ or TiO₂ [14–16]. Using a Pt-dispersed SiO₂-based RRAM device as an example, resistance of the as-fabricated device was increased after operation with darkening the top electrode, whereas the encapsulated device showed an unchanged resistance without physical changes [8,16].

The chemical reactivity between the electrode and the resistive switching material influences the electrical properties of the device [17–19]. The electronic barrier at the metal/insulator interface is formed by the presence of high concentrations of interface states. Therefore, the interfacial states greatly determine device properties. Furthermore, the resistance of RRAM devices is highly dependent on the oxygen affinity of the top electrode. Therefore, to assess the stability of AlN-based RRAM, the effects of moisture/oxygen and electrode materials must be considered.

In this study, AlN-based RRAM devices were fabricated with various top electrode materials (such as Al, Ti, TiN, and Pt) and encapsulated in a thin Al₂O₃ layer to prevent degradation. Time-dependent changes in the electrical characteristics of the RRAM devices were observed for 7

* Corresponding author.

E-mail address: bjchoi@seoultech.ac.kr (B.J. Choi).

weeks. The effects of moisture and electrode materials with or without the encapsulation layer were studied.

2. Experimental

To examine the effect of moisture and top electrode materials, devices were fabricated using four different top electrodes (TE; Al, Ti, TiN, and Pt) with an Al₂O₃ encapsulation layer. Sputter-grown TiN (100 nm) was used as the bottom electrode on a thermally grown SiO₂ layer on a Si wafer. The AlN film was deposited using thermal atomic layer deposition (ALD; Atomic Classic, CN-1, Korea). Trimethyl aluminum (TMA; UP-Chemical, Korea) and NH₃ were used as the precursors of Al and the reactant, respectively. The substrate temperature was maintained at 335 °C. Further details regarding the deposition procedure and film characteristics can be found in the literature [20]. The AlN film was deposited for 38 cycles to a thickness of 7.3 ± 0.5 nm on TiN (4.4 ± 0.4 nm AlN on Si substrate), as measured by an ellipsometer (FS-1, Film-Sense, USA). TEs were grown via physical vapor deposition using a shadow mask with a diameter of 200 μm on the AlN/TiN. The Al TE layer was deposited using a thermal evaporator. The Ti, TiN, and Pt TE layers were deposited via DC magnetron sputtering using Ti, TiN, and Pt targets, respectively. Half of the devices were encapsulated with a 2-nm-thick Al₂O₃ layer via thermal ALD using TMA and H₂O at 250 °C.

Electrical properties were measured at room temperature (~25 °C) using a semiconductor parameter analyzer (SPA; HP-4155A, Agilent, USA). A DC voltage bias was applied to the top electrode, while the bottom electrode was grounded. A schematic diagram of the AlN-based RRAM device structure with an Al₂O₃ encapsulation layer and electrical measurements are shown in Fig. 1 (a). The devices were tested over time from the as-fabricated state for 7 weeks to examine device stability. After electrical measurements for 7 weeks, cross-sections of the devices were prepared using focused ion beam (FIB; Nova 200, FEI, Netherlands) using Ga⁺ ions, and microscopic imaging and elemental mapping were subsequently performed by scanning transmission electron microscopy (STEM; JEM-2100F, JEOL, Japan) and energy dispersive X-ray spectroscopy (EDS). Fig. 1 (b) shows a TEM image of a representative device cross-section composed of a uniformly deposited AlN film with TiN top and bottom electrodes.

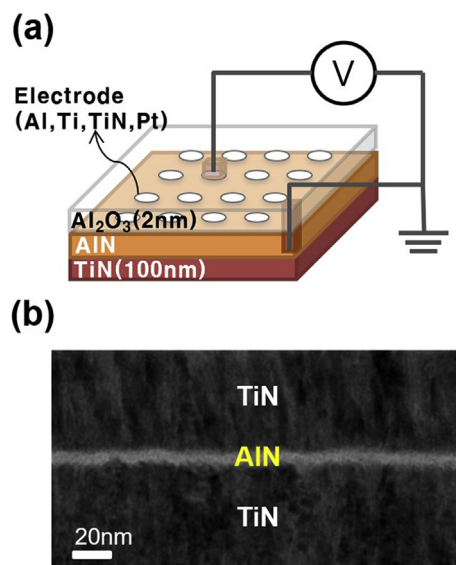


Fig. 1. (a) The schematic diagram of device structure of AlN based RRAM with Al₂O₃ encapsulation layer and electrical measurement system, and (b) TEM image of the cross-section of the device made of uniformly deposited AlN film with TiN top and bottom electrodes.

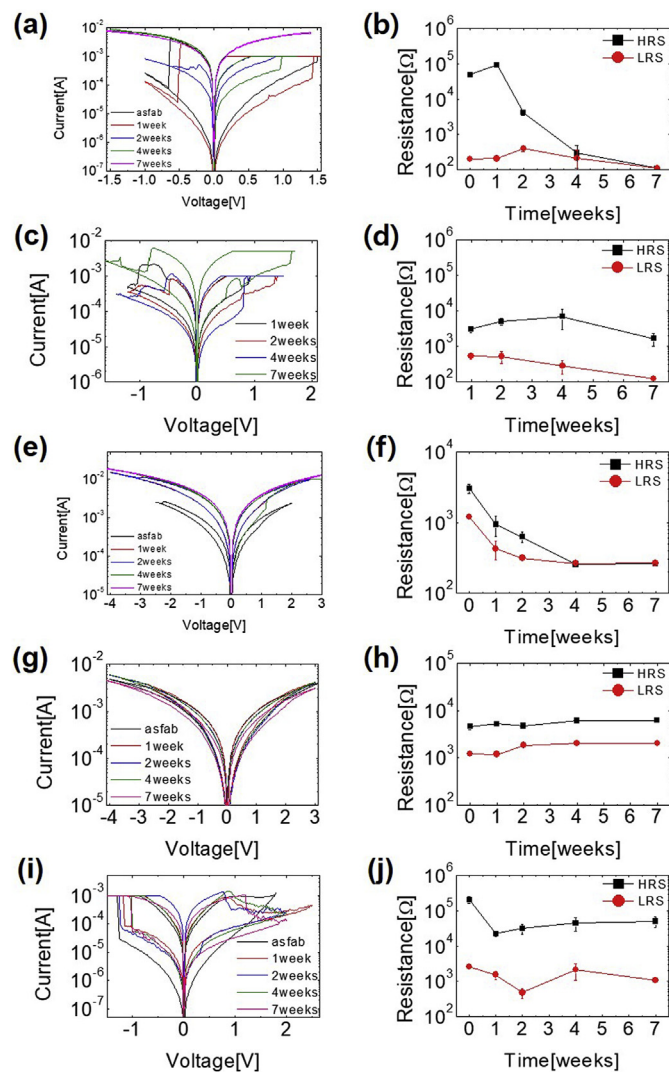


Fig. 2. The I-V loops with time and variation in the resistance states of the device with (a) (b) Al, (c) (d) Al with encapsulation, (e) (f) Ti, (g) (h) TiN, and (i) (j) Pt TEs.

3. Results and discussion

All devices induced the resistive switching phenomena after preconditioning, the so called electroforming (EF) process. The EF process is a soft breakdown process that is achieved by applying electric stimuli to form a conducting filament by creating vacancies in the insulating layer. Generally, EF can occur when oxygen ions escape from the oxide layer involved in the reduction process at the metal/oxide interface [3,21]. Similarly, nitrogen ions play the same role in the nitride layer in nitride-based RRAM devices [3,13]. Once the RRAM devices are electroformed, they show reversible resistive switching phenomena. DC current-voltage (I-V) switching loops and high-resistance state (HRS) and low-resistance state (LRS) were traced up to 7 weeks after fabrication by reading the current at +0.2 V.

Fig. 2(a) and (b) show the I-V loops and variation in the resistance states as a function of time of the device with Al TE without encapsulation. The as-fabricated device showed a high resistance ratio (>10³) at the beginning. However, over time the HRS abruptly decreased 2 weeks after fabrication. The device eventually did not perform a switching loop, maintaining an LRS-stuck state after 4 weeks. This dramatic change could be mitigated using a thin Al₂O₃ encapsulation layer, as shown in Fig. 2(c) and (d). The resistive switching and resistance ratio (~10) were retained for 7 weeks. However, the

encapsulation layer was ineffective because the I-V loops became unstable over time and the resistance decreased compared to that of the initial state. Current compliance was set as low as possible, but a high compliance current (> 1 mA) was required to set the device after 7 weeks. Thus, a high compliance current could be an additional strategy for lowering device resistance.

I-V switching loops and variation in the resistance states of the devices composed of Ti, TiN, and Pt TE are shown in Fig. 2(e)–(j) for the unencapsulated devices. It should be noted that the devices with Ti and TiN TE were formed and set switching (transitioning from HRS to LRS) at a positive bias on the TE similar to that of the device with an Al TE, while the Pt TE device was operated using the opposite bias polarity. In general, more inert metal/nitride interfaces are responsible for the switching similar to the inert metal/oxide interface [4,5,17]. Therefore, AlN/TiN (in case of Al, Ti, and TiN TE) and Pt/AlN interfaces are considered to be switchable inert interfaces based on their switching polarity.

Interestingly, time-dependent degradation differed significantly depending on the device. For devices with a Ti TE (Fig. 2(e) and (f)), although the resistance ratios were smaller than those of the devices with an Al TE, their resistance states decreased. After 4 weeks, the device remained LRS-stuck, whereas a small resistance ratio was maintained and stable resistive switching loops were observed after 7 weeks in the device with a TiN TE, as shown in Fig. 2(g) and (h). The LRS resistance decreased slightly after 2 weeks, but the resistance ratio was maintained for 7 weeks. When a Pt TE was used, reversed I-V switching loops with high resistance ratios (> 10) were obtained and the resistance states were maintained after 7 weeks, as shown in Fig. 2(i) and (j). HRS resistance decreased by approximately 10-fold after 1 week, but it did not degrade further compared to that of the as-fabricated state.

The stability of the resistance states was examined in the devices with various TEs without encapsulation. For this retention test, the as-fabricated and 7-week-old devices were set to HRS and LRS, respectively. The resistance values of the devices read at $+0.2$ V are shown in Fig. 3(a)–(d). These retention characteristics were consistent with the DC I-V measurement results. For the device with an Al TE, the resistance was maintained in the as-fabricated state, but both LRS and HRS resistances decreased after 7 weeks. The device with a Ti TE could not maintain the resistance states observed in the as-fabricated state. Similar to that of the Al TE, the resistances decreased after 7 weeks. However, the devices prepared with TiN and Pt TEs showed robust retention properties even after 7 weeks. For the device containing a TiN TE, the HRS and LRS resistance values slightly decreased after 7 weeks, whereas increased resistance values of both states were observed in the device containing a Pt TE. However, this increased resistance was

induced by the increased reset switching voltage rather than degradation.

The DC I-V measurements and retention test showed that the device with an Al TE showed significant degradation over time. Encapsulation relieved the resistance reduction, but it could not completely prevent degradation. Meanwhile, inert electrode materials such as TiN and Pt preserved the switching properties irrespective of encapsulation. Therefore, moisture did not significantly degrade the properties of the devices and stability of the nitride/metal interface seemed to be more important [4,5,17]. Moisture may accelerate degradation at the interface of an active metal (Al or Ti) and nitride.

To further study the stability and physicochemical changes of the nitride/metal interface, STEM and EDS analyses were performed. Cross-sections of the devices with Al and TiN TEs were prepared by FIB. Fig. 4(a) and (b) show cross-sectional images of the device with an Al/AlN stack. A 6.8-nm-thick uniform AlN layer was formed on TiN BE and partially crystallized phases were confirmed by the high-resolution TEM image and selected area electron diffraction (SAED), as shown in Fig. 4(b) and its inset. Fig. 4(c) and (d) show the cross-sectional images of the device with a TiN/AlN/TiN stack. Similarly, a partially crystallized region was observed in the 7.8-nm-thick AlN layer, as confirmed by the high-resolution image and SAED. Therefore, microstructural differences in the film were not observed in TEM analysis.

In contrast, EDS analysis revealed that the oxygen concentrations significantly differed at the nitride/metal electrode interface. Significant amounts (≥ 20 at%) of oxygen were incorporated into both devices, as shown in Fig. 4(e) and (f). Approximately 16 at% of the oxygen content was incorporated in the AlN film grown at 335°C , as determined by X-ray photoelectron spectroscopy [20]. The elemental depth profile revealed that the oxygen concentration was lower than 5 at%, as confirmed by Auger electron spectroscopy. Therefore, high oxygen concentration originated owing to the introduction of external moisture or collection of internal oxygen during device operation. Specifically, the oxygen concentration in the Al/AlN/TiN device stack was highest near the interface of the Al/AlN, reaching almost 40 at%. In contrast, the oxygen concentration at the top interface of TiN/AlN was approximately 16 at% in the TiN/AlN/TiN device stack, similar to that observed in the film itself. Therefore, the high initial oxygen content in the Al electrode is drawn to the oxygen-deficient Al/AlN interface and oxidized AlN layer during device operation. However, the TiN/AlN interface is less oxygen-deficient and less reactive initially, rendering it more oxidation-resistant. This, it is apparent that the oxygen concentration and reactivity of the top electrode and the film affect the device reliability [19,22,23].

To investigate the relationship between degradation and reactivity with oxygen, the resistance ratio (R_{HRS}/R_{LRS}) and oxide formation energy were considered. Fig. 5 (a) shows the variation in the resistance ratio of devices fabricated with various electrode materials. The resistance ratio changed in the devices with Al and Ti TEs. In contrast, the resistance was largely unchanged in the devices fabricated with TiN and Pt TEs. Assuming that the degradation level (R_{degra}) is directly related to the degree of resistance ratio change, it can be expressed as the following equation:

$$R_{\text{degra}} = \frac{\log(R_{\text{ratio},0}) - \log(R_{\text{ratio},7})}{\log(R_{\text{ratio},0})} \times 100(\%)$$

where R_{ratio,0} and R_{ratio,7} represent the resistance ratio of the as-fabricated and 7-week-old devices, respectively, and R_{degra} is determined by comparison with the Gibbs free energy of oxide formation in Fig. 5 (b) [24]. Larger free energies of oxide formation result in increased degradation of the resistance ratio.

Valov et al. reported the effects of oxygen and moisture in Ta₂O₅- and HfO₂-based systems, as determined by electrical and cyclic voltammetry measurements under controlled oxygen partial pressure and humidity [10]. Moisture was incorporated at the metal/oxide interface

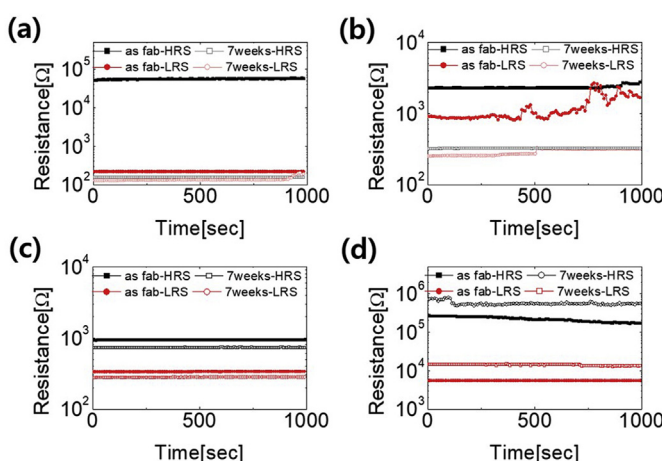


Fig. 3. The resistance values of as-fabricated and 7-week-passed devices read at $+0.2$ V with (a) Al, (b) Ti, (c) TiN, and (d) Pt TEs for retention test.

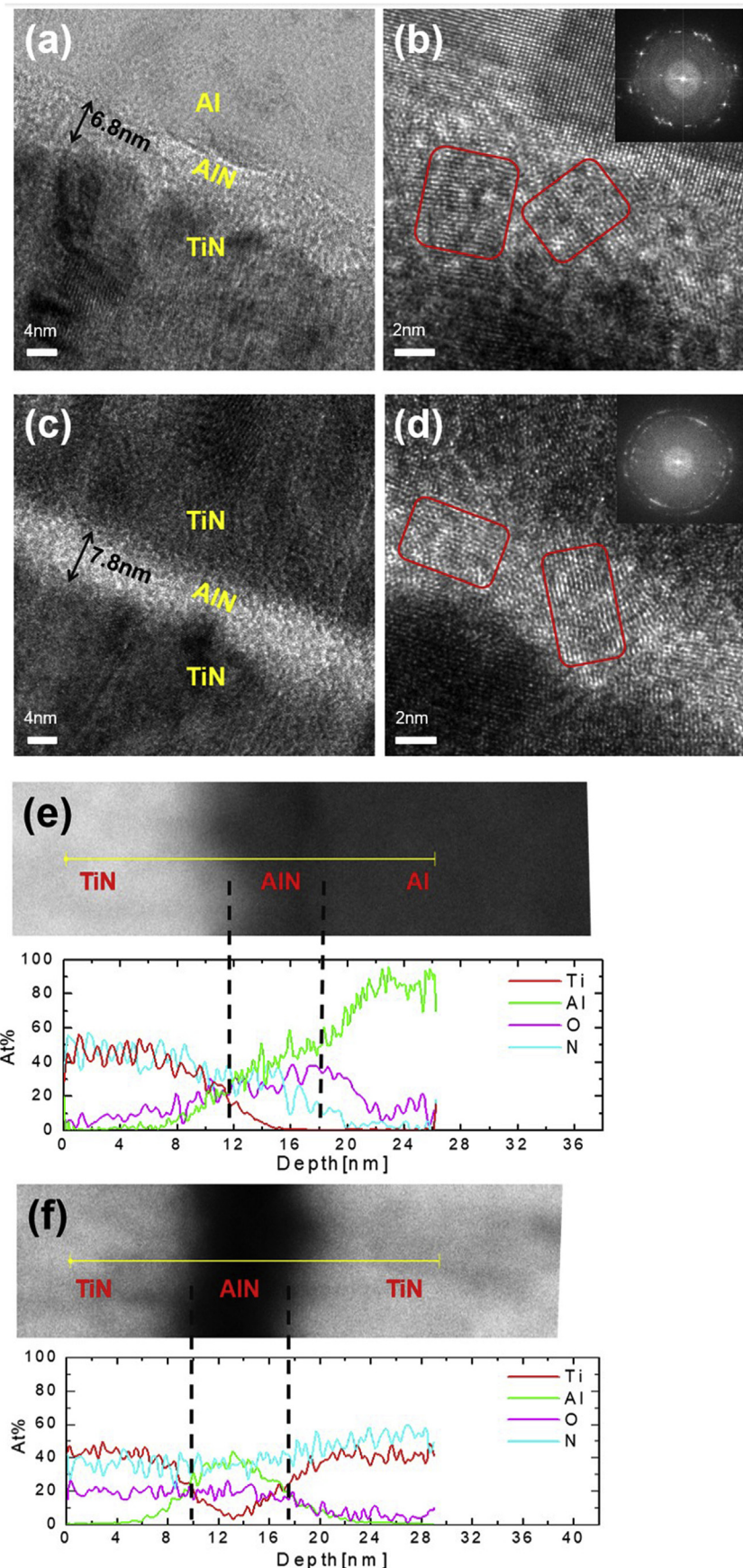


Fig. 4. The cross-sectional TEM images of the device with (a) (b) Al/AlN/TiN and (c) (d) TiN/AlN/TiN stacks, respectively. Inset figures of (b) and (d) are the SAED showing partially crystallized phases. Elemental line profiles of (e) Al/AlN/TiN and (f) TiN/AlN/TiN stack by EDS analysis.

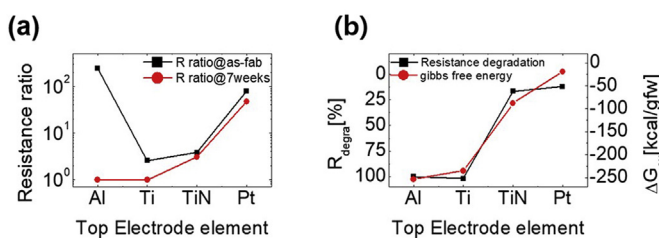


Fig. 5. (a) The variation in the resistance ratio of the devices with various electrode materials and (b) Rdegra of devices with the TE materials comparing with the Gibbs free energy of oxide formation.

by the reduction reaction, which results in easier EF with lower voltages and increased total conductivity owing to the formation of charged ionic species (e.g., OH⁻). The authors also showed that oxygen affects neither the electrochemical reactions nor the EF/switching processes. However, this is not exactly the same for the nitride system used in this work.

Moisture can be incorporated at the metal/nitride interface by reduction to form hydrogen gas and hydroxyl (OH⁻) ions, similar to the process that occurs at the metal/oxide interface. In addition, oxygen incorporation into the AlN film is also expected since the bond dissociation energy of Al–O (481 ± 21 kJ/mol at 0 K) is much higher than that of Al–N (297 kJ/mol at 0 K) or Al–Al (188 ± 42 kJ/mol at 0 K) [5]. Oxygen-related defects such as neutral O_N⁰ or positively charged O_N⁺ in AlN do not lead to enhanced electrical conduction because of their deep energy levels. However, incorporated oxygen that replaces nitrogen can provide additional mobile nitrogen ions, which may enhance ionic motion, facilitating the EF process. Therefore, nitrogen vacancies are readily generated by removing N from AlN via oxygen incorporation and transporting it to the reactive metal electrode at the metal/nitride interface.

In contrast, water molecule incorporation may lead to the hydrolysis of the AlN layer [25,26], resulting in the formation of Al(OH)₃ and charged ions (NH₄⁺ and OH⁻) locally around the conducting filament at elevated temperatures during the switching process. Thereby, moisture could oxidize the AlN layer and provide charged ions to further react with the reactive metal layer. Because of the high reactivity of the electrode materials used herein, rejuvenation of nitrogen vacancies does not occur even when a high voltage is applied. Conversely, more inert electrode materials such as TiN and Pt do not readily react with the charged ions and instead act as an ionic reservoir, facilitating maintenance of the resistance and switching properties of the device.

4. Conclusion

AlN-based RRAM devices were fabricated, and their degradation properties were examined for 7 weeks. To prevent degradation of the resistance and resistive switching of the Al/AlN/TiN stack, encapsulation in a 2-nm-thick Al₂O₃ layer and various top electrode materials (Ti, TiN, and Pt) were tested. Encapsulation slowed the degradation of the device, while the top electrode metal more significantly affected the degradation properties regardless of the encapsulation status. With inert electrode materials such as TiN and Pt, the device retained resistance values and switching properties compared to devices with Al and Ti TEs. Oxygen and moisture could be incorporated at the interface of metal/nitride and the reaction of moisture with AlN could result in AlN film hydrolysis during operation. Charged ions (OH⁻ and NH₄⁺) react with the metal layer, degrading the resistance and resistive switching properties of the device. The degradation mechanism and its prevention using certain electrode materials and encapsulation will be practically useful for the realization of RRAM and associated derivatives for embedded memory, logic-in-memory, and synaptic devices in neuromorphic computing.

Acknowledgments

This research was supported by Basic Science Research Program through the National Research Foundation of Korea (NRF), funded by the Ministry of Education (2017R1D1A1A09000809).

References

- [1] R. Waser, R. Dittmann, G. Staikov, K. Szot, Redox-based resistive switching memories - nanoionic mechanisms, prospects, and challenges, *Adv. Mater.* 21 (2009) 2632–2663, <https://doi.org/10.1002/adma.200900375>.
- [2] L. Chua, Resistance switching memories are memristors, *Appl. Phys. A* 102 (2011) 765–783, <https://doi.org/10.1007/s00339-011-6264-9>.
- [3] Z. Zhang, B. Gao, Z. Fang, X. Wang, Y. Tang, J. Sohn, H.-P. Wong, S.S. Wong, G. Lo, All-metal-nitride RRAM devices, *IEEE Electron. Device Lett.* 36 (2015) 29–31, <https://doi.org/10.1109/LED.2014.2367542>.
- [4] B.J. Choi, J.J. Yang, M.-X. Zhang, K.J. Norris, D. a. a. Ohlberg, N.P. Kobayashi, G. Medeiros-Ribeiro, R.S. Williams, Nitride memristors, *Appl. Phys. A* 109 (2012) 1–4, <https://doi.org/10.1007/s00339-012-7052-x>.
- [5] B.J. Choi, A.C. Torrezan, J.P. Strachan, P.G. Kotula, A.J. Lohn, M.J. Marinella, Z. Li, R.S. Williams, J.J. Yang, High-speed and low-energy nitride memristors, *Adv. Funct. Mater.* 26 (2016) 5290–5296, <https://doi.org/10.1002/adfm.201600680>.
- [6] A.M. Emel'yanov, Water-related charge carrier traps in thermal silicon dioxide films prepared in dry oxygen, *Phys. Solid State* 52 (2010) 1131–1137, <https://doi.org/10.1134/S1063783410060041>.
- [7] T. Tsuruoka, K. Terabe, T. Hasegawa, I. Valov, R. Waser, M. Aono, Effects of moisture on the switching characteristics of oxide-based, gapless-type Atomic switches, *Adv. Funct. Mater.* 22 (2012) 70–77, <https://doi.org/10.1002/adfm.201101846>.
- [8] X. Yang, B.J. Choi, A.B.K. Chen, I.W. Chen, Cause and prevention of moisture-induced degradation of resistance random access memory nanodevices, *ACS Nano* 7 (2013) 2302–2311, <https://doi.org/10.1021/nn3054544>.
- [9] T. Heisig, C. Baeumer, U.N. Gries, M.P. Mueller, C. La Torre, M. Luebben, N. Raab, H. Du, S. Menzel, D.N. Mueller, C.L. Jia, J. Mayer, R. Waser, I. Valov, R.A. De Souza, R. Dittmann, Oxygen exchange processes between oxide memristive devices and water molecules, *Adv. Mater.* 30 (2018) 1800957, <https://doi.org/10.1002/adma.201800957>.
- [10] M. Lübben, S. Wiefels, R. Waser, I. Valov, Processes and effects of oxygen and moisture in resistively switching TaOx and HfO_x, *Adv. Electron. Mater.* 4 (2018) 1700458, <https://doi.org/10.1002/aelm.201700458>.
- [11] T. Mattila, R. Nieminen, Ab initio study of oxygen point defects in GaAs, GaN, and AlN, *Phys. Rev. B* 54 (1996) 16676–16682, <https://doi.org/10.1103/PhysRevB.54.16676>.
- [12] M. Kazan, B. Ruffl, C. Zgheib, P. Masri, Oxygen behavior in aluminum nitride, *J. Appl. Phys.* 98 (2005) 5–8, <https://doi.org/10.1063/1.2137461>.
- [13] K.F. T.I. D Spassov, A. Paskaleva, Effect of oxygen concentration and metal electrode on the resistive switching in MIM capacitors with transition metal oxides, *J. Phys. Conf. Ser.* 794 (2017) 012016, <https://doi.org/10.1088/1742-6596/755/1/011001>.
- [14] A.A. Dameron, S.D. Davidson, B.B. Burton, P.F. Garcia, R.S. McLean, S.M. George, Gas diffusion barriers on polymers using multilayers fabricated by Al 2 O 3 and rapid SiO 2 atomic layer deposition, *J. Phys. Chem. C* 112 (2008) 4573–4580.
- [15] P.F. Garcia, R.S. McLean, M.D. Groner, a. a. Dameron, S.M. George, Gas diffusion ultrabarriers on polymer substrates using Al₂O₃/Si₃N₄ plasma-enhanced chemical vapor deposition, *J. Appl. Phys.* 106 (2009) 023533, <https://doi.org/10.1063/1.3159639>.
- [16] B.J. Choi, I.W. Chen, Effects of moisture barriers on resistive switching in Pt-dispersed SiO₂ nanometallic thin films, *Appl. Phys. A Mater. Sci. Proc.* 112 (2013) 235–239, <https://doi.org/10.1007/s00339-013-7776-2>.
- [17] J.J. Yang, J.P. Strachan, F. Miao, M.X. Zhang, M.D. Pickett, W. Yi, D. a. a. Ohlberg, G. Medeiros-Ribeiro, R.S. Williams, Metal/TiO₂ interfaces for memristive switches, *Appl. Phys. Mater. Sci. Process* 102 (2011) 785–789, <https://doi.org/10.1007/s00339-011-6265-8>.
- [18] C. Chen, S. Gao, F. Zeng, G.S. Tang, S.Z. Li, C. Song, H.D. Fu, F. Pan, Migration of interfacial oxygen ions modulated resistive switching in oxide-based memory devices, *J. Appl. Phys.* 114 (2013) 014502, <https://doi.org/10.1063/1.4812486>.
- [19] N. Ge, M.-X. Zhang, L. Zhang, J.J. Yang, Z. Li, R.S. Williams, Electrode-material dependent switching in TaOx memristors, *Semicond. Sci. Technol.* 29 (2014) 104003, <https://doi.org/10.1088/0268-1242/29/10/104003>.
- [20] Y. Kim, M.S. Kim, H.J. Yun, S.Y. Ryu, B.J. Choi, Effect of growth temperature on AlN thin films fabricated by atomic layer deposition, *Ceram. Int.* 44 (2018) 17447–17452, <https://doi.org/10.1016/j.ceramint.2018.06.212>.
- [21] D. Ielmini, Resistive switching memories based on metal oxides: mechanisms, reliability and scaling, *Semicond. Sci. Technol.* 31 (2016) 1–25, <https://doi.org/10.1088/0268-1242/31/6/063002>.
- [22] T. Kim, G. Baek, S. Yang, J.Y. Yang, K.S. Yoon, S.G. Kim, J.Y. Lee, H.S. Im, J.P. Hong, Exploring oxygen-affinity-controlled TaN electrodes for thermally advanced TaOx bipolar resistive switching, *Sci. Rep.* 8 (2018) 1–9, <https://doi.org/10.1038/s41598-018-26997-y>.
- [23] M. Lanza, H.S.P. Wong, E. Pop, D. Ielmini, D. Strukov, B.C. Regan, L. Larcher, M.A. Villena, J.J. Yang, L. Goux, A. Belmonte, Y. Yang, F.M. Puglisi, J. Kang, B. Magyari-Köpe, E. Yalon, A. Kenyon, M. Buckwell, A. Mehonie, A. Shluger, H. Li, T.H. Hou, B. Hudacek, D. Akinwande, R. Ge, S. Ambrogio, J.B. Roldan, E. Miranda,

- J. Suñe, K.L. Pey, X. Wu, N. Raghavan, E. Wu, W.D. Lu, G. Navarro, W. Zhang, H. Wu, R. Li, A. Holleitner, U. Wurstbauer, M.C. Lemme, M. Liu, S. Long, Q. Liu, H. Lv, A. Padovani, P. Pavan, I. Valov, X. Jing, T. Han, K. Zhu, S. Chen, F. Hui, Y. Shi, Recommended methods to study resistive switching devices, *Adv. Electron. Mater.* 5 (2019) 1800143, <https://doi.org/10.1002/aelm.201800143>.
- [24] S.M. Howard, Standard gibb's energies of formation for, *J. Soc. Chem. Ind. (London)*, 63 (1971) 125.
- [25] S. Fukumoto, T. Hookabe, H. Tsubakino, Hydrolysis behavior of aluminum nitride in various solutions, *J. Mater. Sci.* 35 (2000) 2743–2748, <https://doi.org/10.1023/A:1004718329003>.
- [26] R.S. Kumar, U.S. Hareesh, P. Ramavath, R. Johnson, Hydrolysis control of alumina and AlN mixture for aqueous colloidal processing of aluminum oxynitride, *Ceram. Int.* 37 (2011) 2583–2590, <https://doi.org/10.1016/j.ceramint.2011.04.131>.